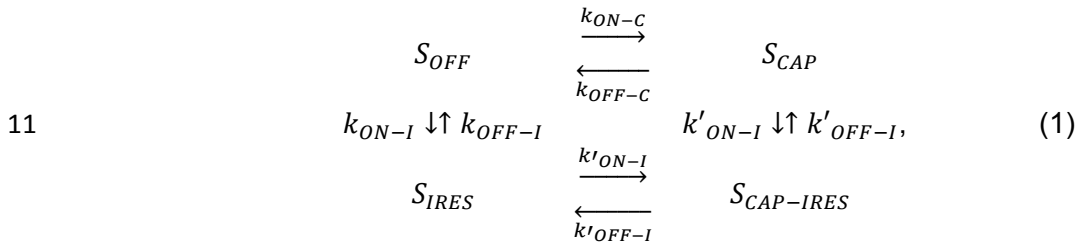


1 **Supplementary Note 1. Computational Details.**

2 A stochastic model was implemented to simulate Cap and IRES activation, ribosome  
 3 initiation, elongation, termination, and potential ribosome recycling mechanisms for cap-  
 4 dependent and IRES-mediated genes.

5 In the mathematical model, initiation events are dictated by the mRNA state. Specifically,  
 6 four possible mRNA activation states were proposed ( $S_{OFF}$ ,  $S_{CAP}$ ,  $S_{IRES}$ ,  $S_{CAP-IRES}$ ), where:  $S_{OFF}$   
 7 represents a non-permissive initiation state;  $S_{CAP}$  allows for only cap-dependent ribosomal  
 8 initiation;  $S_{IRES}$  allows for only IRES-mediated initiation; and  $S_{CAP-IRES}$  allows both cap-  
 9 dependent and IRES-mediated initiation. Eq. 1 represents the transition reactions between  
 10 mRNA states.



12 where each  $k_x$  represents a first-order transition rate between two RNA states, and  $k'_x$  is the  
 13 transition rate conditioned on the activation state of the other construct (e.g.,  $k'_{ON-I}$  is the cap-  
 14 dependent activation rate of IRES). A simpler three-state model was considered by removing  
 15 the fourth RNA state (i.e.,  $S_{CAP-IRES}$ ). The parameter estimation section describes how a system  
 16 with three or four mRNA states was chosen.

17 When the system is in one of the appropriate mRNA activity states, cap-dependent and  
 18 IRES-mediated initiation events occur with propensities  $w_{INIT-C}$  and  $w_{INIT-I}$ , respectively, which  
 19 are defined:

$$w_{INIT-C} = \begin{cases} k_{INIT-C}, & \text{if } S_{CAP} \text{ or } S_{CAP-IRES} , \\ 0, & \text{otherwise,} \end{cases} \quad (2)$$

$$w_{INIT-I} = \begin{cases} k_{INIT-I}, & \text{if } S_{IRES} \text{ or } S_{CAP-IRES}, \\ 0, & \text{otherwise,} \end{cases} \quad (3)$$

22

23 where  $k_{INIT-C}$  and  $k_{INIT-I}$  represent the cap and IRES initiation rates, respectively.

24 To simulate the model under stochastic dynamics, Eqs. (2) and (3) were used to  
 25 generate a vector of random initiation event times for each gene,  $\tau_{INIT_{IRES}}$  and  $\tau_{INIT_{CAP}}$ . A  
 26 codon-dependent model for translation was used, in which the elongation rate for each codon is  
 27 given by  $\bar{k}_e(u_i/\bar{u})$ , where  $u_i$  is the known frequency of the  $i^{th}$  codon in the human genome,  $\bar{u}$  is  
 28 the average codon usage frequency in the human genome, and  $\bar{k}_e$  is the basal elongation rate  
 29 (to be estimated from the data). In the models, the final codon termination rates were assumed  
 30 to be equal to the average elongation rate.

31 For increased computational efficiency, ribosome elongation was approximated using a  
 32 coarse-grained procedure. For this, sparse ribosome loading was assumed to enable simple  
 33 calculation of the average time needed by a ribosome to complete gene elongation,  $\tau_{ke}$ , as  
 34 follows:

$$\tau_{ke} = \sum_{i=1}^L \frac{1}{\bar{k}_e(u_i/\bar{u})}, \quad (4)$$

36 where  $L$  represents the gene length in codons. Using the specific gene sequence for the cap-  
 37 dependent gene and IRES-mediated gene, we calculated the total elongation time  $\tau_{CAP}$  and  
 38  $\tau_{IRES}$ , respectively. At any time,  $t$ , such that  $0 < t - \tau_{INIT_{CAP}} < \tau_{CAP}$ , the position of a given cap-  
 39 translating ribosome was obtained by calculating the proportion of elongated gene as follows:

$$x_{CAP} = j \text{ such that } \sum_{i=1}^j \frac{1}{\bar{k}_e(u_i/\bar{u})} \leq t - \tau_{INIT_{CAP}} < \sum_{i=1}^{j+1} \frac{1}{\bar{k}_e(u_i/\bar{u})}, \quad (5)$$

40

41 and for the IRES-mediated gene for  $0 < t - \tau_{INIT_{IRES}} < \tau_{IRES}$ :

42 
$$x_{IRES} = j \text{ such that } \sum_{i=1}^j \frac{1}{\bar{k}_e \left( \frac{u_i}{\bar{u}} \right)} \leq t - \tau_{INIT_{IRES}} < \sum_{i=1}^{j+1} \frac{1}{\bar{k}_e \left( \frac{u_i}{\bar{u}} \right)}, \quad (6)$$

43 where  $\tau_{INIT_{CAP}}$  and  $\tau_{INIT_{IRES}}$  are the times at which the corresponding ribosome initiated  
44 translation begins.

45 To consider potential interaction mechanisms between cap-dependent and IRES-  
46 mediated translation, two possible hypotheses were postulated:

47 A first hypothetical model considers potential ribosome recycling (or crossover)  
48 mechanisms, by which a ribosome that completes translation of the cap-dependent gene could  
49 immediately re-initiate translation of the IRES-mediated gene. In this context, a new  
50 propensity,  $w_{CI}$ , that specifies the probability that a ribosome completing cap will re-initiate at  
51 IRES was introduced. The specification of such reactions reflects single-mRNA translation  
52 observations by Wang et al., 2016<sup>1</sup>, which suggest ribosome hops between adjacent open  
53 reading frames on a single RNA. To test if such recycling mechanisms are necessary to  
54 reproduce the experimental data, multiple models with and without nonzero values for the  
55 crossover rate  $w_{IC}$  were compared.

56 In the second hypothetical model, cap and IRES interdependency were tested by  
57 assuming that the activation and deactivation of cap or IRES could depend on the activity state  
58 for the other sensor (e.g., IRES could activate faster when cap is already active). Including  
59 different combinations of these hypothetical mechanisms in the three- and four-state models led  
60 us to propose a list of 14 different sub-models, each comprising between 7 and 12 free  
61 parameters (see Extended Data Fig. 6b). The sub-models test different hypotheses, including  
62 variations of the number of mRNA states (3 or 4 states), dependency on Cap and IRES  
63 switching states, and/or the existence of the cross-over mechanism. Cap and IRES dependency

64 are represented in the see Extended Data Fig. 6b by red lines, which denote that the  
65 corresponding reaction parameter value has a free value during the optimization process. All  
66 models have 3 or 4 mRNA states, denoted by 3S or 4S, respectively. From see Extended Data  
67 Fig. 6b left to right, the first seven models lack crossover, while the last seven have cross-over  
68 (denoted by subscript 'C', e.g. 3SC). Models can have independent (denoted by subscript 'I') or  
69 dependent (denoted by subscript 'D') Cap or IRES activation/deactivation. Models can also  
70 have a single dependent activation or deactivation rate (denoted by subscript 'm1' or 'm2').

### 71 ***Converting ribosome elongation times to fluorescence intensity***

72 To relate the ribosome elongation times to fluorescence intensity, a similar approach as  
73 in Aguilera et al.<sup>2</sup> was adopted. Ribosome occupancy is converted to fluorescence intensity by  
74 increasing the simulated intensity by one unit after each ribosome moves across the tag-region.  
75 For this, a cumulative *probe design vector* was defined that records the number of probe sites  
76 upstream from each codon,  $\mathbf{c}_g = [c_1, c_2, \dots, c_L]$ , for the appropriate construct (i.e.,  $g = \text{cap-}$   
77 dependent or IRES-mediated genes, respectively). Using this, the intensity was calculated as  
78 the sum of the product of the position of the ribosome at a given time and  $\mathbf{c}_g$ . For cap-  
79 dependent spots, the intensity vector is defined as:

$$80 \quad I_{CAP}(t) = \sum \mathbf{c}_{CAP}(\mathbf{x}_{CAP}(t)), \quad (8)$$

81 and for IRES-mediated spots it is:

$$82 \quad I_{IRES}(t) = \sum \mathbf{c}_{IRES}(\mathbf{x}_{IRES}(t)), \quad (9)$$

83 where  $\mathbf{c}_g(\mathbf{x}_g)$  is the intensity of a given ribosome at position  $\mathbf{x}_g$ , and the summations are taken  
84 over all ribosomes present on the mRNA at time  $t$ . To have consistent units of intensity between  
85 model simulations and experimental data, intensity values are reported in units of mature  
86 proteins (u.m.p.) as described in detail on the Methods section.

## 87 **Comparison of experimental data and model**

88 To reproduce experimental data, the model was simulated using a modified Direct  
89 Method<sup>3</sup> for 4000 trajectories representing independent RNA spots. Simulations were run for a  
90 burn-in period of 10,000 seconds to approximate steady state. Simulations were processed and  
91 used to capture spot intensity for the cap-dependent gene ( $I_{CAP}$ ) and the IRES-mediated gene  
92 ( $I_{IRES}$ ). Additionally, simulated spots were classified as cap-dependent with probability  $P_{CAP}$ ,  
93 IRES-mediated with probability  $P_{IRES}$ ; both with probability  $P_{CAP-IRES}$ , or neither with probability  
94  $P_{None}$ .

## 95 **Modeling Harringtonine experiments**

96 Harringtonine inhibits new initiation events by directly blocking the 60S subunit in the  
97 ribosome, and it has been widely used to perform run-off assays to estimate elongation rates.<sup>4</sup>  
98 To mimic the effects of Harringtonine in our model, the initiation rate was modified for the first  
99 gene as follows:

$$100 \quad w_{INIT-C} = \begin{cases} k_{INIT-C}, & \text{if } t < t_H, \\ 0, & \text{otherwise,} \end{cases} \quad (10)$$

101 and the initiation rate for the second gene as follows:

$$102 \quad w_{INIT-I} = \begin{cases} k_{INIT-I}, & \text{if } t < t_H, \\ 0, & \text{otherwise,} \end{cases} \quad (11)$$

103 where  $t_H$  is the time of application of Harringtonine.

## 104 **Modeling Sodium Arsenite (NaAs) and Dithiothreitol (DTT) experiments**

105 NaAs and DTT are chemical stresses that have been used to affect cap-dependent  
106 initiation in previous single-molecule translation experiments.<sup>1</sup> The mechanism of action for  
107 NaAs is not well understood, but it has been suggested to affect ribosome initiation through its

108 action on translation factors, such as eIF2a and eIF4.<sup>5</sup> To simulate these chemical stresses, two  
 109 potential mechanisms of action were tested. The first potential mechanism of action involves  
 110 blocking cap-dependent translation by affecting its RNA state, and was implemented in the  
 111 model by modifying the cap activation rates,  $k_{ON-C}$  and  $k'_{ON-C}$ , as follows:

$$112 \quad k_{ON-C} = \begin{cases} k_{ON-C}, & \text{if } t < t_{ST}, \\ k_{ST} \cdot k_{ON-C}, & \text{otherwise,} \end{cases} \quad (12)$$

113 and

$$114 \quad k'_{ON-C} = \begin{cases} k'_{ON-C}, & \text{if } t < t_{ST}, \\ k_{ST} \cdot k'_{ON-C}, & \text{otherwise,} \end{cases} \quad (13)$$

115 where,  $k_{ST}$  is an inhibition constant, where a total inhibition is achieved by  $k_{ST} = 0$ , and a null  
 116 inhibition is achieved by  $k_{ST} = 1$ . The time  $t_{ST}$  denotes the time of stress application.

117 In the second mechanism of action, it was hypothesized that the drug directly blocks  
 118 cap-dependent translation initiation. In the model, this is achieved by modifying  $w_{ini}$  as follows:

$$119 \quad w_{INIT-C} = \begin{cases} k_{INIT-C}, & \text{if } t < t_{ST}, \\ k_{ST} \cdot k_{INIT-C}, & \text{otherwise.} \end{cases} \quad (14)$$

## 120 **Parameter estimation and optimization routines**

121 The parameter estimation strategy consists of finding a parameter set ( $\bar{\Lambda}$ ) that  
 122 statistically reproduces all experimental data, including intensity histograms, fractions of  
 123 translating spots, and Harringtonine ribosomal run-off assays as follows:

### 124 **Intensity histograms**

125 To compare experimental and simulated steady-state intensity histograms, the  
 126 probability to observe the experimentally determined intensities ( $d^{cap}$  or  $d^{IRES}$ ) was estimated

127 given a parameter set  $(\Lambda)$  in the model implementation. To estimate  $P(d; \Lambda)$ , histograms were  
 128 collected using  $N_t = 4000$  independent stochastic trajectories per parameter evaluation. The  
 129 likelihood function was estimated as follows:

$$130 \quad L_{Dist}(D|M) = \prod_{j=1}^{N_D} P(d_j; \Lambda), \quad (15)$$

131 and the log-likelihood as:

$$132 \quad \log L_{Dist}(D|M) = \sum_{j=1}^{N_D} \log P(d_j; \Lambda), \quad (16)$$

133 where  $D$  represents the data measured in  $N_D$  independent experimental data, and  $M$   
 134 corresponds to the model. As the experimental measurements can only detect protein  
 135 intensities above a threshold of one mature protein, all spots with intensities below 1 u.m.p.  
 136 were defined as non-translating mRNA. This metric was applied to experimental data consisting  
 137 of cap-dependent spots (CAP) and IRES-mediated spots (IRES). With this, a total log-likelihood  
 138 function was calculated as the sum of the functions for cap and IRES spots, that is:

$$139 \quad \log L_{T_{Dist}}(D|M) = \sum_{j=1}^{N_t} \log P_{CAP}(d_j^{cap}; \Lambda) + \sum_{j=1}^{N_t} \log P_{IRES}(d_j^{IRES}; \Lambda). \quad (17)$$

#### 140 ***Fraction of translating spot***

141 A similar approach was used to compute the likelihood to observe the experimentally  
 142 determined number of spots classified as Cap-only, IRES-only, Cap+IRES, and non-translating.  
 143 The likelihood function was computed as follows:

$$144 \quad L_F(D|M) = \prod_{j=1}^{N_D} P(f_j; \Lambda), \quad (18)$$

145 and the log-likelihood as:

$$146 \quad \log L_F(D|M) = \sum_{j=1}^{N_D} \log P(f_j; \Lambda) = \sum_i N_i \log P(f_i; \Lambda), \quad (19)$$

147 where each  $f_j$  denotes the type (i.e., Cap, IRES, Cap+IRES, or non-translating) of the  $j^{th}$  spot,  
 148  $N_D$  is the total number of independent observed spots,  $N_i$  is the number of independent  
 149 observed spots of the  $i^{th}$  type, and  $P(f_j; \Lambda)$  is the categorical distribution of spots of each type  
 150 estimated by the model simulations with parameters  $\Lambda$ .

### 151 ***Harringtonine induced ribosomal run-off***

152 To compare simulated and experimental time course data representing the intensity after  
 153 Harringtonine application, a Gaussian likelihood function was assumed and calculated as  
 154 follows:

$$155 \quad L_{HT}(I_D | I_M) = \prod_{i=1}^{N_D} \frac{1}{\sqrt{2\pi\sigma(t_i)^2}} \exp\left(-\frac{(I_D(t_i) - I_M(t_i; \Lambda))^2}{2\sigma(t_i)^2}\right), \quad (20)$$

156 with a log-likelihood form given by:

$$157 \quad \log L_{HT}(I_D | I_M) = C_{HT} - \sum_{i=1}^{N_D} \frac{(I_D(t_i) - I_M(t_i; \Lambda))^2}{2\sigma(t_i)^2}, \quad (21)$$

158 where  $\sigma(t_i)$  is approximated by the measured SEM, and  $N_D$  is the number of time points from  
 159 the Harringtonine run-off curve. In this log-likelihood formulation,  $C_{HT}$  is a constant that doesn't  
 160 depend on the parameters.

161 Experimental data was quantified for the total intensities for cap ( $I_{CAP-D}$ ) and IRES  
 162 ( $I_{IRES-D}$ ) within all spots (after subtraction of the base level of intensity). These two data sets  
 163 were collected to compute a total log-likelihood function as follows:

$$164 \quad \log L_{THT}(I_D | I_M) = \log L_{HT_{CAP}}(I_{CAP-D} | I_M) + \log L_{HT_{IRES}}(I_{IRES-D} | I_M). \quad (22)$$

165 Parameter searches consisted of optimization routines based on genetic algorithms (GA) using  
 166 the function *ga* in MATLAB. The optimization routine was implemented with a population of 100  
 167 individuals for 30 generations, and the implementation was run multiple times with random initial



168 conditions. Additionally, the Pattern Search Algorithm<sup>6</sup> was implemented using the function  
169 *patternsearch* in MATLAB to ensure convergence. The best parameter values were selected by  
170 minimizing a global objective function that considers all data sets, that is:

$$171 \quad -\log L_{Total}(D|M) = -(\log L_{T_{Dist}}(D|M) + \log L_F(D|M) + \log L_{T_{HT}}(I_D|I_M)). \quad (23)$$

172 The comparison of the optimization results for all tested models is given in Extended Data Fig.  
173 6c-d.

### 174 ***Assessing how well models predict Sodium Arsenite (NaAs) and Dithiothreitol (DTT)*** 175 **experiments**

176 After optimizing the models, cross-validation experiments were predicted using the  
177 chemical stresses, NaAs and DTT. For this, simulated and experimental time course data  
178 representing the total translation spot intensity after NaAs or DTT application were compared.  
179 The likelihood function was calculated as follows:

$$180 \quad L_{ST}(I_D|I_M) = \prod_{i=1}^{N_D} \frac{1}{\sqrt{2\pi\sigma(t_i)^2}} \exp\left(-\frac{(I_D(t_i)-I_M(t_i;\Lambda))^2}{2\sigma(t_i)^2}\right), \quad (24)$$

181 and the log-likelihood function is:

$$182 \quad \log L_{ST}(I_D|I_M) = C_{ST} - \sum_{i=1}^{N_D} \frac{(I_D(t_i)-I_M(t_i;\Lambda))^2}{2\sigma(t_i)^2}, \quad (25)$$

183 where  $\sigma(t_i)$  is approximated by the measured SEM, and  $N_D$  is the number of time points  
184 measured in the drug-treatment curve, and  $C_{ST}$  is constant that doesn't depend on model  
185 parameters.

186 For chemical stress experiments, three data sets were used representing the intensity  
187 for Cap-only spots, IRES-only spots, and green (Cap) intensity in both cap and IRES spots.  
188 These three data sets were considered on a total log-likelihood function as follows:

189  $-\log L_{T_{ST}}(I_D|I_M) = -(\log L_{ST_{CAP}}(I_{CAP-D}|I_M) + \log L_{ST_{IRES}}(I_{IRES-D}|I_M) + \log L_{ST_{CI}}(I_{Cap+IRES-D}|I_M)).$   
190 (26)

### 191 **Uncertainty Quantification**

192 To quantify uncertainty, the best parameter set from fitting was initially used and 100  
193 runs of 1,000 step Markov Chain Monte Carlo (MCMC) algorithm were run to explore an  
194 additional 100,000 possible parameter combinations. At each step, a random perturbation of  
195 10% to the current parameters was proposed, and every proposal for which the log-likelihood  
196 for the new parameter set was within a 1% of that found for the best fit was accepted (i.e., all  
197 parameters for which  $\log(L(I_D|I_{Best})/L(I_D|I_{New})) < 60$  were accepted). The standard deviation  
198 of the resulting 26,650 accepted parameter sets was then used as a measure of parameter  
199 uncertainty as shown in Table 1.

### 200 **Computational Implementation and Codes**

201 All simulations were performed on the W. M. Keck High Performance Computing Cluster at  
202 Colorado State University. All codes and required data are available at:  
203 [https://github.com/MunskyGroup/Koch\\_Aguilera\\_etal\\_2020.git](https://github.com/MunskyGroup/Koch_Aguilera_etal_2020.git).

### 204 **Supplementary Note References**

- 205 1. Wang, C., Han, B., Zhou, R. & Zhuang, X. Real-Time Imaging of Translation on Single mRNA  
206 Transcripts in Live Cells. *Cell* **165**, 990–1001 (2016).
- 207 2. Aguilera, L. U. *et al.* Computational design and interpretation of single-RNA translation  
208 experiments. *PLOS Comput. Biol.* **15**, e1007425 (2019).
- 209 3. Gillespie, D. T. A general method for numerically simulating the stochastic time evolution of  
210 coupled chemical reactions. *J. Comput. Phys.* **22**, 403–434 (1976).
- 211 4. Morisaki, T. *et al.* Real-time quantification of single RNA translation dynamics in living cells.  
212 *Science* **352**, 1425–1429 (2016).

213 5. Holcik, M. & Sonenberg, N. Translational control in stress and apoptosis. *Nat. Rev. Mol. Cell*  
214 *Biol.* **6**, 318–327 (2005).

215 6. HookeRobert & A, J. `` Direct Search'' Solution of Numerical and Statistical Problems. *J.*  
216 *ACM JACM* (1961).

217

218

219